Mechanical loading reveals cell type-specific responses and role of PHGDH in endothelial cell growth

Sakari Mäntyselkä[1*], Erik Niemi[1*], Laura Ylä-Outinen[1], Kalle Kolari[1], Liina Uusitalo-Kylmälä[1], Alfredo Ortega-Alonso[1], Roosa-Maria Liimatainen[2], Vasco Fachada[1], Perttu Permi[2,3,4], Elina Kalenius[2], Juha J Hulmi[1#], Riikka Kivelä[1,5,6#]

[1]Faculty of Sport and Health Sciences, NeuroMuscular Research Center, University of Jyväskylä, Jyväskylä, Finland
[2]Department of Chemistry, University of Jyväskylä, Jyväskylä, Finland
[3]Department of Biological and Environmental Science, University of Jyväskylä, Jyväskylä, Finland
[4]Institute of Biotechnology, Helsinki Institute of Life Science, University of Helsinki, Helsinki, Finland
[5]Stem Cells and Metabolism Research Program, Research Programs Unit, Faculty of Medicine, University of Helsinki, Helsinki, Finland
[6]Wihuri Research Institute, Helsinki, Finland

* Equal contribution as first authors

# Equal contribution as senior authors

Correspondence to Riikka Kivelä (riikka.m.kivela@jyu.fi) & Juha J Hulmi (juha.hulmi@jyu.fi), NeuroMuscular Research Center, Faculty of Sport and Health Sciences, University of Jyväskylä, Rautpohjankatu 8, 40014 Finland

Keywords

Acetate/Cell-stretching/Exercise/Muscle/Serine

Abstract

Skeletal muscle and blood vessels are constantly subjected to mechanical forces, especially during exercise. We subjected human endothelial cells (ECs) and muscle cells (MCs) to cyclic mechanical stretch and investigated acute transcriptomic and metabolomic changes. Mechanical loading induced several responses typically seen after exercise in vivo. Both cell types released acetate in response to stretching, but surprisingly, many of the other changes were in opposite directions. For instance, electron transport chain genes were downregulated in ECs and upregulated in muscle cells. Additionally, ECs shifted their transcriptomic profile to a growth-oriented direction and ^{13}C-(U)-glucose tracing experiments revealed increased serine synthesis in ECs. Mechanistic experiments related to the serine synthesis pathway enzyme phosphoglycerate dehydrogenase (PHGDH) revealed its importance in EC anabolism. Our data suggest that mechanical loading induces cell type-specific responses in ECs and MCs, and several of these effects recapitulate exercise effects *in vivo*. In ECs, mechanical loading activates the serine synthesis pathway, and the serine-synthesizing enzyme PHGDH was highlighted as essential in regulating EC growth, a process indispensable in angiogenesis.

Introduction

Skeletal muscle is highly vascularized and myofibers and endothelial cells together make up ~70% of the total nuclei count in skeletal muscle tissue (Englund *et al*, 2021; Pepe & Albrecht, 2023). Myofibers are contractile cells that both produce and sense mechanical forces. Endothelial cells lining the blood vessels sense mechanical forces produced by blood flow (shear stress) and contracting and stretching muscle. In skeletal muscle, mechanical forces are produced and sensed especially during exercise, which can be mimicked *in vitro* using contraction and stretching models (Lautaoja *et al*, 2023). Previously, it has been demonstrated that cyclic mechanical loading (i.e. cyclic stretching) induces a wide variety of molecular and morphological responses in endothelial (reviewed in Jufri *et al*, 2015) and muscle cells (reviewed in Ren *et al*, 2021). For example, mechanical loading has been found to activate the mechanistic target of rapamycin complex 1 (mTORC1) (Nakai *et al*, 2015) and to induce highly similar gene expression changes in myofiber-like multinucleated cells (myotubes) as resistance exercise *in vivo* in myofibers (Turner *et al*, 2021). Endothelial cells, in turn, have been shown to orient in a 60-70° angle relative to the direction of stretch, secrete angiocrines, and activate angiogenesis-related pathways (Große-Segerath *et al*, 2024; Jufri *et al*, 2015; Lorenz *et al*, 2018), which also occur in response to exercise and increased blood flow *in vivo* (Biernat *et al*, 2024; Sottiurai *et al*, 1989). However, there are only a few studies (Große-Segerath *et al*, 2024; Hinkle *et al*, 2022; Ilaiwy *et al*, 2016) investigating the remodeling of the global molecular landscape in response to mechanical loading, and none in comparing responses in different cell types. It is recently acknowledged that endothelial and muscle cell cross-talk is essential in regulating the development, maintenance, and repair of muscle tissue (reviewed in Pepe & Albrecht, 2023).

Skeletal muscle responses to mechanical loading *in vivo* have mostly been examined using mixed muscle samples, which lack cell-specificity as skeletal muscle contains over 10 different cell types (Englund *et al*, 2021). *In vitro* models allow us to study the metabolic responses in a cell type-specific manner. However, according to our knowledge, there are no studies in which mechanical loading-induced responses of muscle and endothelial cells have been compared. Exercise induces many metabolic changes such as increased glycolysis and oxidative phosphorylation in the whole muscle level (Smith *et al*, 2023). However, little is known about how exercise or mechanical loading *per se* affects other metabolic pathways such as those branching from glycolysis (e.g., the pentose phosphate and serine synthesis pathways), and their role in exercise responses such as angiogenesis. Previously, mechanical stretching of liver endothelial cells during vasodilation was demonstrated to induce angiocrine signals that support liver growth and survival, and potentially contribute to liver regeneration (Lorenz *et al*, 2018). Blood vessels in skeletal muscles experience immediate vasodilation—and thus endothelial cell stretching—when their physiological function is extensively needed during exercise.

Here we mechanically loaded two different human endothelial cell lines and primary human skeletal muscle cells to mimic exercise on-a-dish and to study cell type-specific responses. Transcriptomics and metabolomics analyses revealed unique

oxidative and glycolytic changes in these two cell types in response to mechanical loading. Further mechanistic experiments identified the serine synthesis pathway activation, and specifically phosphoglycerate dehydrogenase (PHGDH), as an essential driver of endothelial cell anabolism.

Results

Mechanical loading induced transcriptomic changes in all cell types and altered exercise-related and mechanosensitive gene expression

We first investigated the transcriptomic changes in two different types of human endothelial cell lines (HUVEC & HCMEC) as well as human skeletal muscle cells (HSkM) (Fig. 1A). The mechanical loading did not induce detachment of the cells, significant membrane damage, or cell death in either muscle or endothelial cells as determined by total RNA yield and the extracellular lactate dehydrogenase (LDH) activity assay (Supplementary Fig. 1A-B). Based on the differential gene expression analysis, we found that all three cell types presented significant changes in their transcriptome in response to the mechanical loading, as demonstrated by the principal component analysis (PCA) (Fig. 1B). The transcriptomic response was the largest in HUVECs, with the total number of differentially expressed genes being approximately 3-fold larger than in HCMECs or HSkM cells (Fig. 1C).

In HUVECs, 717 genes were upregulated, and 779 genes were downregulated ($\log_2$FC ≥ 0.5 & adj. p ≤ 0.05). By indexing genes in order of magnitude and consistency of change ($\log_2$FC and adj. p), the five most significantly upregulated protein-coding genes were *STC1*, *ADAM19*, *INSR*, *AKAP12* and *GUCY1A1*. The five most significantly downregulated protein-coding genes by the same indexing were H2-4 clustered histones *H3C12*, *H4C9*, *H3C8*, *H3C13* and *H2AC16*. In HCMECs, 241 genes were upregulated, and 261 genes were downregulated. The five most significantly upregulated protein-coding genes were *KITLG*, *ITGB8*, *FGF5*, *FBXO30* and *SLC7A11* and, similarly to HUVECs, the five most significantly downregulated ones were again H2-4 clustered histones *H4C9*, *H3C12*, *H4C6* and *H2BC7,* as well as H1.3 linker histone *H1-3*. A total of 388 genes in HSkM cells were differentially expressed, from which 262 genes were upregulated and 126 genes were downregulated in response to mechanical loading. The five most significantly upregulated protein-coding genes were *THBD, IL11, GPRC5A, SNAI1* and *RASD1* and the five most significantly downregulated protein-coding genes were *CCN1, CCN2*, *RGS4*, *DLC1* and *F3*. For the complete lists of differentially expressed genes and their full names, please refer to Supplementary Table S1.

Moreover, when comparing overlaps in both up- and downregulated genes in all three cell lines, we noticed that the two endothelial cell lines clearly showed similarities in their gene expression, whereas the overlaps in gene expression between endothelial cells and muscle cells were small (Fig. 1E). Only one gene was

upregulated (*CREB5*) in all three cell lines and similarly, only one gene was downregulated (*FAM43A*) in all three cell lines in response to mechanical loading. For the complete lists of overlapping differentially expressed genes, please refer to Supplementary Table S2. These results demonstrated greater transcriptomic responses to mechanical loading in endothelial cells than in muscle cells. Large overlaps in gene expression could be seen between the endothelial cell lines, whereas endothelial cells and muscle cells responded differently, highlighting the cell type-specificity.

To evaluate the external validity of the model, we next checked the expression of common exercise-induced and mechanosensitive genes. From HSkM cells, we specifically focused on PGC1α encoding gene (*PPARGC1A*) and its upstream regulator PPAR-delta (*PPARD*), myostatin (*MSTN*), *NR4A3, and VEGFA.* We observed, similarly as shown in response to exercise in vivo (Pillon *et al*, 2020; Hood *et al*, 2016; Fan & Evans, 2015; Wickramasinghe *et al*, 2022; Smith *et al*, 2024; Hulmi *et al*, 2007; Kim *et al*, 2005), upregulation of *PPARD*, *NR4A3*, and *VEGFA,* downregulation of *MSTN*, while no change in *PPARGC1A* (Supplementary Fig. 2A). From endothelial cells, we examined the gene expression of common mechanosensitive genes *KLF2/4*, *THDB*, *NRP2*, *YAP1*, *HIF1A*, NRF2 encoding gene (*NFE2L2*) (Li *et al*, 2024; Davis *et al*, 2023; Peng *et al*, 2019) as well as *FLT1*, *KDR* and *FLT4* which are genes encoding for VEGF receptors 1/2/3. We found that all except *HIF1A* and *FLT4* were statistically significantly upregulated in HUVECs (Supplementary Fig. 2B-C). In HCMECs none of the changes in these genes reached statistical significance. In addition, we inspected the expression of selected mechanotransduction genes that have been linked to angiogenesis in endothelial cells (Nan *et al*, 2023). These genes included the VE-cadherin-encoding gene (*CDH5*), and eight other genes (*CTNND1*, *CTNNA1, CTNNB*1, *SRC*, *PTPRB*, *PTPRJ*, *PTPRM*, and *JUP*) related to VE-cadherin. We found that the gene expression of α- and β-catenin coding genes *CTNNA1* and *CTNNB1* significantly increased in HUVECs. We also observed that the expression of genes coding p120 (adj. p = 0.055), VE-PTP (adj. p = 0.07), and VE-Cadherin (adj. p = 0.08) tended to increase (Supplementary Fig. 2D). Together, these findings suggest that our *in vitro* mechanical loading model mimics exercise-related mechanical stress.

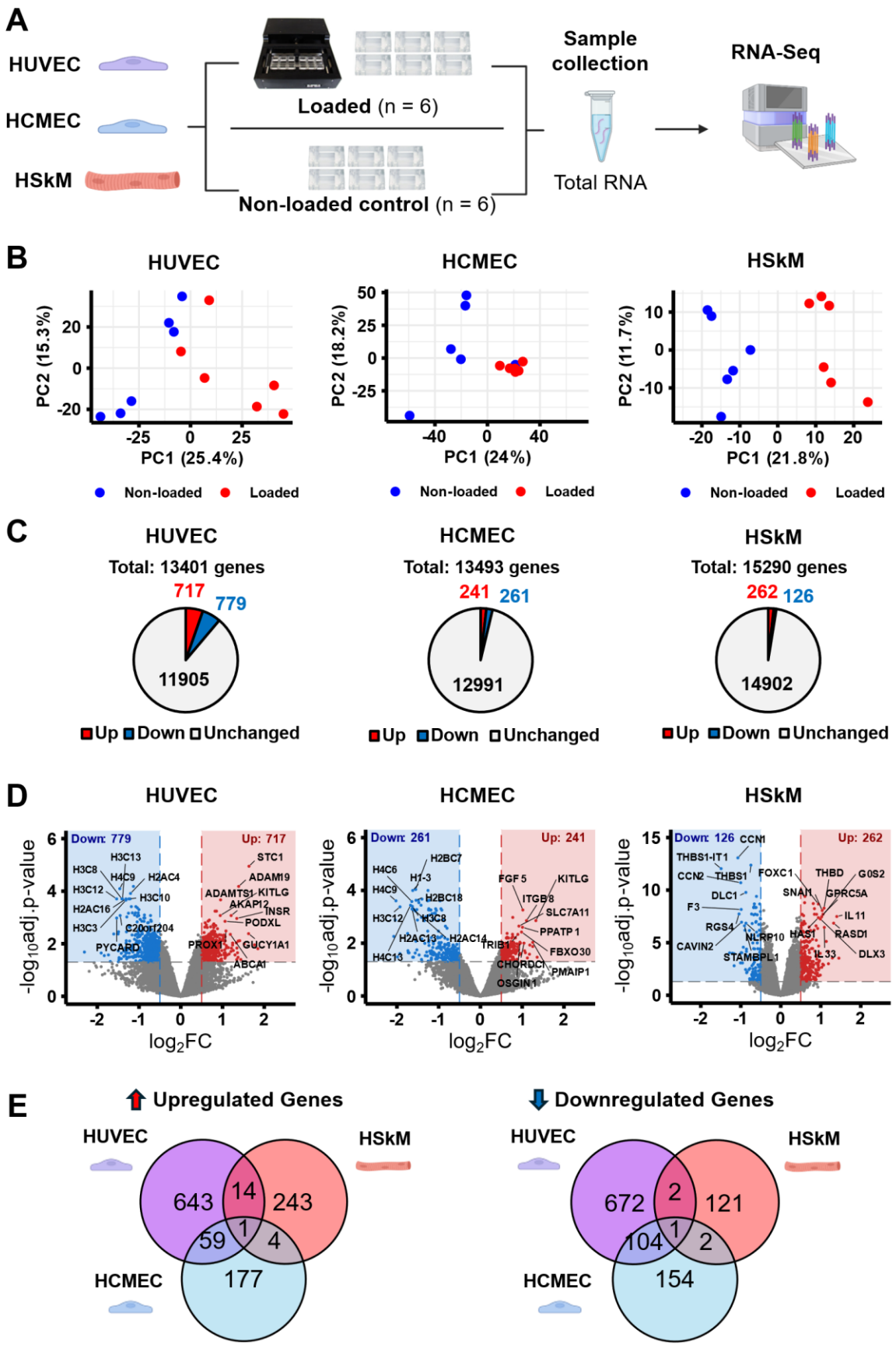

Fig. 1 Changes in gene expression of human endothelial cells (HUVECs, HCMECs) and muscle cells (HSkM) in response to mechanical loading. **A)** Schematic representation of

experimental design. The experiment was repeated for each cell line separately. Cells from one stretching chamber were used as one sample for RNA-Seq. **B)** PCA plots of samples in each cell line respectively. **C)** The total number of detected genes and the number of genes that were either up- or downregulated ($\log_2$FC ≥ 0.5 and adj. $p \leq 0.05$) for each cell line. **D)** Volcano plots illustrating the amounts of differentially expressed and unchanged genes in all three cell lines. Top 10 up- and downregulated genes by magnitude and consistency are annotated **E)** Venn diagrams showing the number of shared up- and downregulated genes in all three cell lines

Mechanical loading resulted in cell type-specific transcriptomic responses

Gene Set Enrichment Analysis (GSEA) results revealed (Supplementary Table S3) that the two endothelial cell lines showed highly similar pathway enrichment after mechanical loading. 20 Gene Ontology: Biological Processes (GO:BP) and four Reactome pathways were similarly upregulated in HUVEC and HCMEC, and 27 GO:BP, 83 Reactome and three KEGG pathways were similarly downregulated. Overlaps in pathway enrichment between endothelial cells and muscle cells towards the same direction were seen in the upregulation of only two GO:BP pathways: *Ovulation* and *Ovarian follicle development*. These pathways included TGF-β family genes, which are known to regulate muscle growth. Interestingly, the GSEA results of endothelial cells showed upregulation of cell growth-related pathways such as *Endothelial cell development, RNA-splicing* and *Negative regulation of catabolic processes* (Fig. 2A). Furthermore, both endothelial cell lines showed downregulation of pathways related to *Chromatin remodeling* and *Cellular senescence* (Fig. 2B). For muscle cells, upregulated pathways were mostly related to oxidative phosphorylation and ribosome biogenesis, while pathways related to cell mechanical integrity, such as *Actin organization* and *Cell matrix adhesion*, were downregulated (Fig. 2A-B). Many of the GSEA findings were also reproduced by the gene set overrepresentation analysis (ORA) (Supplementary Fig. 3).

Much to our surprise, when comparing gene set enrichment of the endothelial cell lines to muscle cells, we found multiple pathways enriched in opposite directions in response to mechanical loading (Supplementary Table S4). In HUVECs and HSkM cells 12 GO:BP, three Reactome and two KEGG pathways were oppositely enriched and the same was true for HCMECs and HSkM cells in 14 GO:BP, four Reactome and three KEGG pathways. Most of these pathways were related to cellular respiration, metabolism, electron transport chain (ETC), as well as chromatin remodeling (Fig. 2C). Most prominently, pathways related to oxidative phosphorylation were downregulated in endothelial cell lines, while upregulated in muscle cells. Closer inspection revealed that gene expression in all five mitochondrial ETC-complexes were affected in the same fashion (Fig. 2D).

205

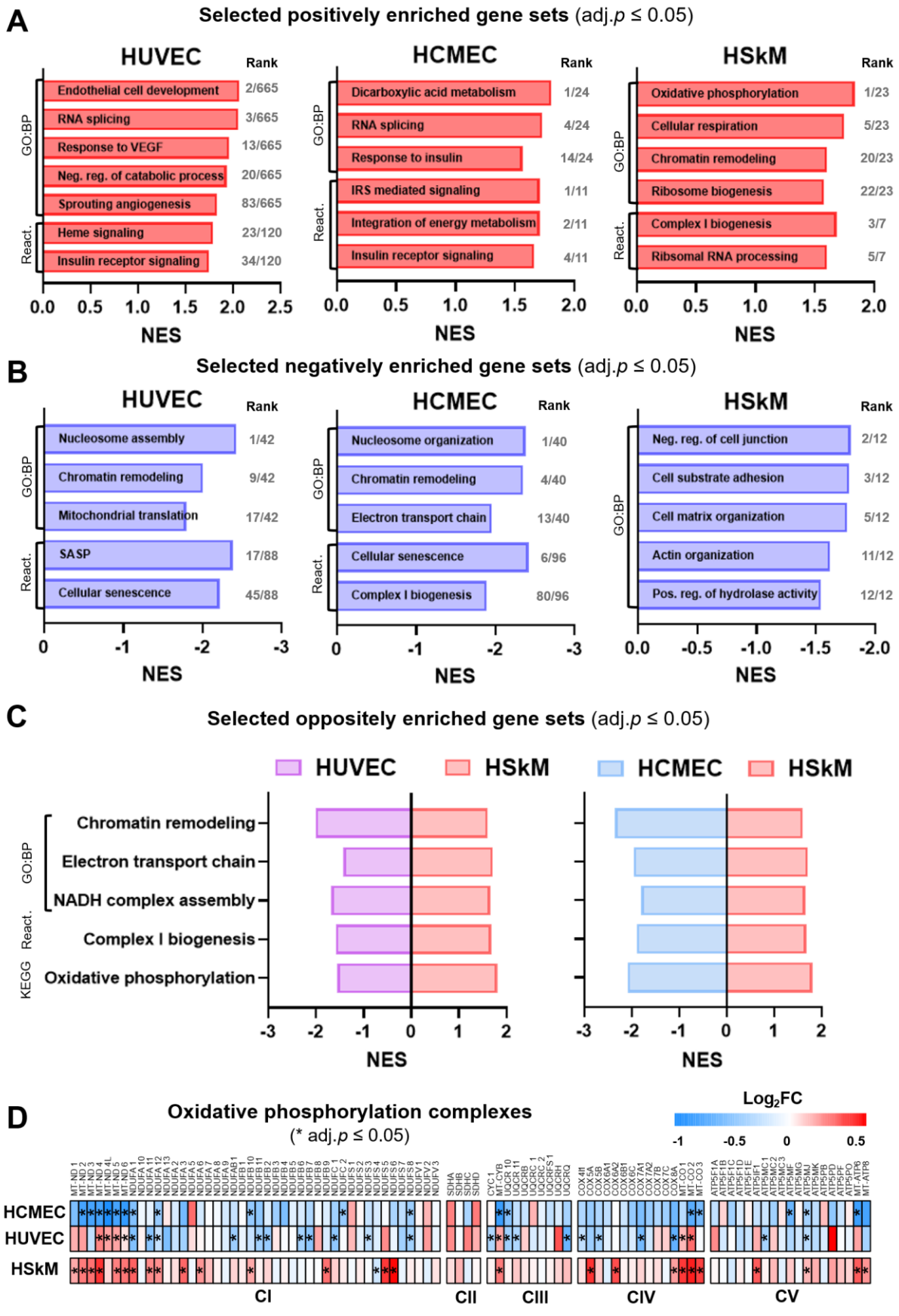
A
Selected positively enriched gene sets (adj.p ≤ 0.05)
HUVEC
Rank
GO:BP
Endothelial cell development 2/665
RNA splicing 3/665
Response to VEGF 13/665
Neg. reg. of catabolic process 20/665
Sprouting angiogenesis 83/665
React.
Heme signaling 23/120
Insulin receptor signaling 34/120
0.0 0.5 1.0 1.5 2.0 2.5
NES
HCMEC
Rank
GO:BP
Dicarboxylic acid metabolism 1/24
RNA splicing 4/24
Response to insulin 14/24
React.
IRS mediated signaling 1/11
Integration of energy metabolism 2/11
Insulin receptor signaling 4/11
0.0 0.5 1.0 1.5 2.0
NES
HSkM
Rank
GO:BP
Oxidative phosphorylation 1/23
Cellular respiration 5/23
Chromatin remodeling 20/23
Ribosome biogenesis 22/23
React.
Complex I biogenesis 3/7
Ribsomal RNA processing 5/7
0.0 0.5 1.0 1.5 2.0
NES
B
Selected negatively enriched gene sets (adj.p ≤ 0.05)
HUVEC
Rank
GO:BP
Nucleosome assembly 1/42
Chromatin remodeling 9/42
Mitochondrial translation 17/42
React.
SASP 17/88
Cellular senescence 45/88
0 -1 -2 -3
NES
HCMEC
Rank
GO:BP
Nucleosome organization 1/40
Chromatin remodeling 4/40
Electron transport chain 13/40
React.
Cellular senescence 6/96
Complex I biogenesis 80/96
0 -1 -2 -3
NES
HSkM
Rank
GO:BP
Neg. reg. of cell junction 2/12
Cell substrate adhesion 3/12
Cell matrix organization 5/12
Actin organization 11/12
Pos. reg. of hydrolase activity 12/12
0.0 -0.5 -1.0 -1.5 -2.0
NES
C
Selected oppositely enriched gene sets (adj.p ≤ 0.05)
HUVEC
HSkM
HCMEC
HSkM
GO:BP
Chromatin remodeling
Electron transport chain
NADH complex assembly
React.
Complex I biogenesis
KEGG
Oxidative phosphorylation
-3 -2 -1 0 1 2
NES
-3 -2 -1 0 1 2
NES
D
Oxidative phosphorylation complexes
(* adj.p ≤ 0.05)
Log2FC
-1 -0.5 0 0.5
HCMEC
HUVEC
HSkM
CI
CII
CIII
CIV
CV

206

Fig. 2 GSEA results of HUVECs, HCMECs and HSkM in response to mechanical loading. **A)** Selected positively enriched gene sets from GO:BP, Reactome and KEGG database terms. **B)** Selected negatively enriched gene sets from GO:BP, Reactome and KEGG database terms. **C)** Gene sets that were systematically downregulated in both endothelial cell lines and upregulated in muscle cells. **D)** Heatmap depicting the gene expression in the oxidative phosphorylation complex genes in response to mechanical loading. NES = Normalized enrichment score. GO:BP = Gene ontology:Biological process. Rank = Rank of gene set by NES in all statistically significant (adj. $p \leq 0.05$) up- or downregulated gene sets in their respective database. SASP = Senescence-associated secretory phenotype

To further compare our results to in vivo exercise, we applied the MetaMEx database (Pillon *et al*, 2020) to examine whether the *Endothelial Cell development* pathway, which was among the most upregulated GO:BP pathways in HUVECs, is commonly induced in response to acute aerobic exercise. Indeed, we found that many of these genes were induced also in human skeletal muscle tissue in response to acute aerobic exercise (Supplementary Fig. 4).

In summary, mechanical loading induced positive enrichment of pathways related to angiogenesis and ribosome biogenesis and changes in typical exercise-regulated genes, suggesting that mechanical loading alone recapitulates several common exercise effects seen *in vivo*. The pathway enrichment results together with the gene expression overlaps of individual genes, further reinforce the cell type-specific responses induced by mechanical loading. This was most prominently seen in the opposite expression of oxidative phosphorylation pathways and ETC genes, which were downregulated in endothelial cells and upregulated in muscle cells.

Mechanical loading resulted in greater metabolite changes in HUVECs compared to HSkM cells

Next, we compared metabolite changes in HUVECs and HSkM cells in response to mechanical loading. The HCMECs were excluded because these analyses required more sample material and resources than transcriptomics. We analyzed a targeted list of intracellular metabolites with UHPLC-MS/MS, and culture media metabolites with non-targeted ^{1}H NMR spectroscopy (Fig. 3A, Supplementary Table S5). In HSkM cells and HUVECs, 3/35 and 11/38 intracellular metabolites were altered in response to mechanical loading, respectively (Fig. 3B). The intracellular metabolite alterations were thus greater in HUVECs than in HSkM cells, which is in line with the transcriptome results. From the conditioned media (i.e., extracellular) metabolites, 3/29 were altered in HSkM cells, and 2/34 in HUVECs (Fig. 3B).

By comparing conditioned media to the media incubated without cells (i.e., cell-free media), we found that both HUVECs and HSkM cells released acetate into the media in response to mechanical loading (Fig. 3C-D). We also confirmed the acetate release into the media with UHPLC-MS (Supplementary Fig. 5). The acetate release results were even more prominent with UHPLC-MS than with ^{1}H NMR (Supplementary Fig. 5A-B). In addition, arginine and glutamine levels were greater in

the media of loaded HSkM cells and pyruvate levels in the media of loaded HUVECs (Fig. 3C-D).

In muscle cells, intracellular levels of glucose 6-phosphate and phosphocreatine were decreased while alanine levels were increased (Fig. 3E). In HUVECs, intracellular levels of phosphoenolpyruvate, fructose 6-phosphate, and α-ketoglutarate were decreased while phosphoserine, serine, asparagine, threonine, proline, alanine, acetyl-CoA, and tryptophan levels increased in response to mechanical loading (Fig. 3F). The two most increased metabolites were phosphoserine and serine (Fig. 3F), while the serine synthesis pathway gene expressions were not affected (Supplementary Fig. 2E). Proline and α-ketoglutarate were the two most consistently (smallest *p*-values) changed metabolites. The observed increase in proline and decrease in α-ketoglutarate may indicate that proline was synthesized using α-ketoglutarate.

Next, we conducted a metabolite overrepresentation analysis using the significantly altered intracellular metabolites. The overrepresentation analysis of HSkM cells did not yield any significant results because of the low number of altered metabolites. In HUVECs, the most enriched pathways were *Glycine and serine metabolism*, *Glutamate metabolism*, and *Warburg effect* (Fig. 3G). These results, together with the decreased gene expression of the electron transport chain complexes and increased gene expression of growth-related pathways, suggest that mechanical stretching may reprogram endothelial cell metabolism towards the Warburg effect and biosynthesis of serine and other amino acids.

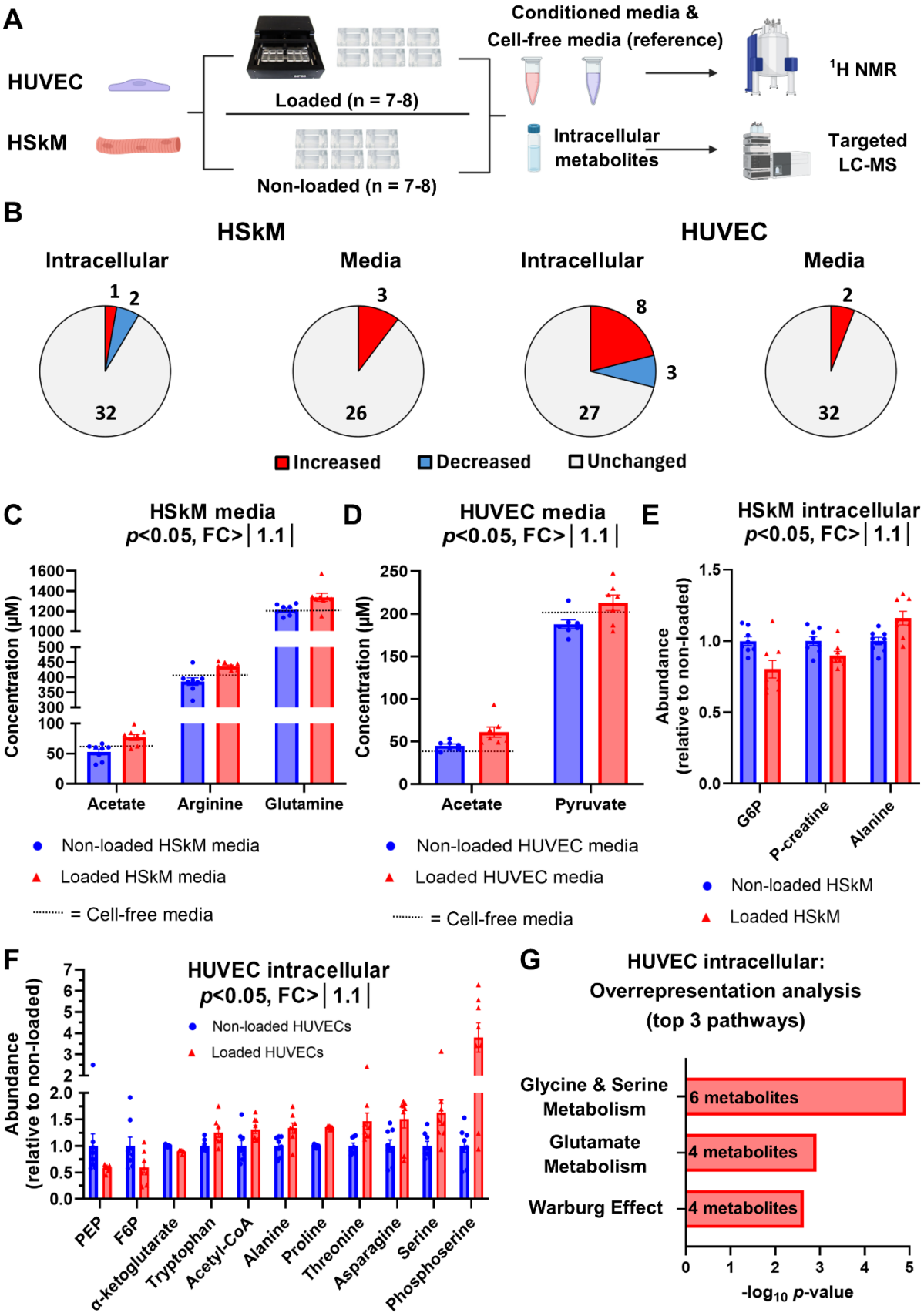

Fig. 3 Intracellular and culture media metabolite changes of human skeletal muscle cells (HSkM) and HUVECs in response to mechanical loading**. A)** Culture media metabolites were analyzed with ^{1}H NMR spectroscopy and intracellular metabolites were analyzed using the

targeted UHPLC-MS/MS method. Cells or media from three stretching chambers were pooled for one sample. Also, media incubated without cells (i.e., Cell-free media) was included as an additional reference. **B)** The number of increased, decreased, and unchanged intracellular and culture media metabolites of HSkM cells and HUVECs. **C)** Significantly changed media metabolites of HSkM cells. **D)** Significantly changed media metabolites of HUVECs. **E)** Significantly changed intracellular metabolites in HSkM cells. **F)** Significantly changed intracellular metabolites in HUVECs. **G)** Metabolite overrepresentation analysis using the significantly altered intracellular metabolites of HUVECs. In panel G, the number of metabolites indicates how many significantly altered metabolites from each pathway were detected. Individual values (n = 7-8 per group) are plotted, and data are presented as mean ± SEM. The dashed lines represent the average concentrations in cell-free media samples. P-creatine = Phosphocreatine, G6P = Glucose 6-phosphate, PEP = Phosphoenolpyruvate, F6P = Fructose 6-phosphate

Mechanical loading increased the synthesis of serine, alanine, and proline from glucose

As serine metabolism was the most highlighted pathway in mechanically loaded HUVECs, we next conducted dynamic labeling experiments with ^{13}C-(U)-glucose (Fig. 4A) to assess if the serine synthesis rate was affected. We found that there were significantly more total (unlabeled + labeled), and newly synthesized serine and phosphoserine at multiple time points after mechanical loading (Fig. 4B-E). This indicates that the serine synthesis was, indeed, increased in response to mechanical loading in HUVECs. There were no significant changes in the total serine level in the media (Fig. 4F), whereas mechanically loaded HUVECs released significantly more labeled serine into the culture media (Fig. 4G), supporting the interpretation that serine synthesis was increased by mechanical loading.

We also assessed if the synthesis of alanine, proline, glycine, aspartate, asparagine, glutamine, glutamate, and arginine were changed. We found that there were also more labeled and total alanine and proline in loaded HUVECs and their media (Supplementary Fig. 6A-G), indicating that alanine and proline synthesis were increased together with serine synthesis in response to mechanical loading.

There was significantly less labeled glycine in loaded HUVECs at 3 h and 20 h time points and total glycine at the 0 h time point (Supplementary Fig. 6H-I), but no differences in labeled or total glycine release into media (Supplementary Fig. 6J-K) compared to non-loaded controls. We did not find significant differences in labeled aspartate and glutamate (Supplementary Fig. 7). In the case of asparagine, arginine, and glutamine, ^{13}C-labeled molecules were not detected after isotope natural abundance correction, suggesting that HUVECs did not use glucose to produce these amino acids in these nutritional conditions (Supplementary Table S6).

Together, these results suggest that mechanical loading increases the synthesis of serine, alanine, and proline in endothelial cells.

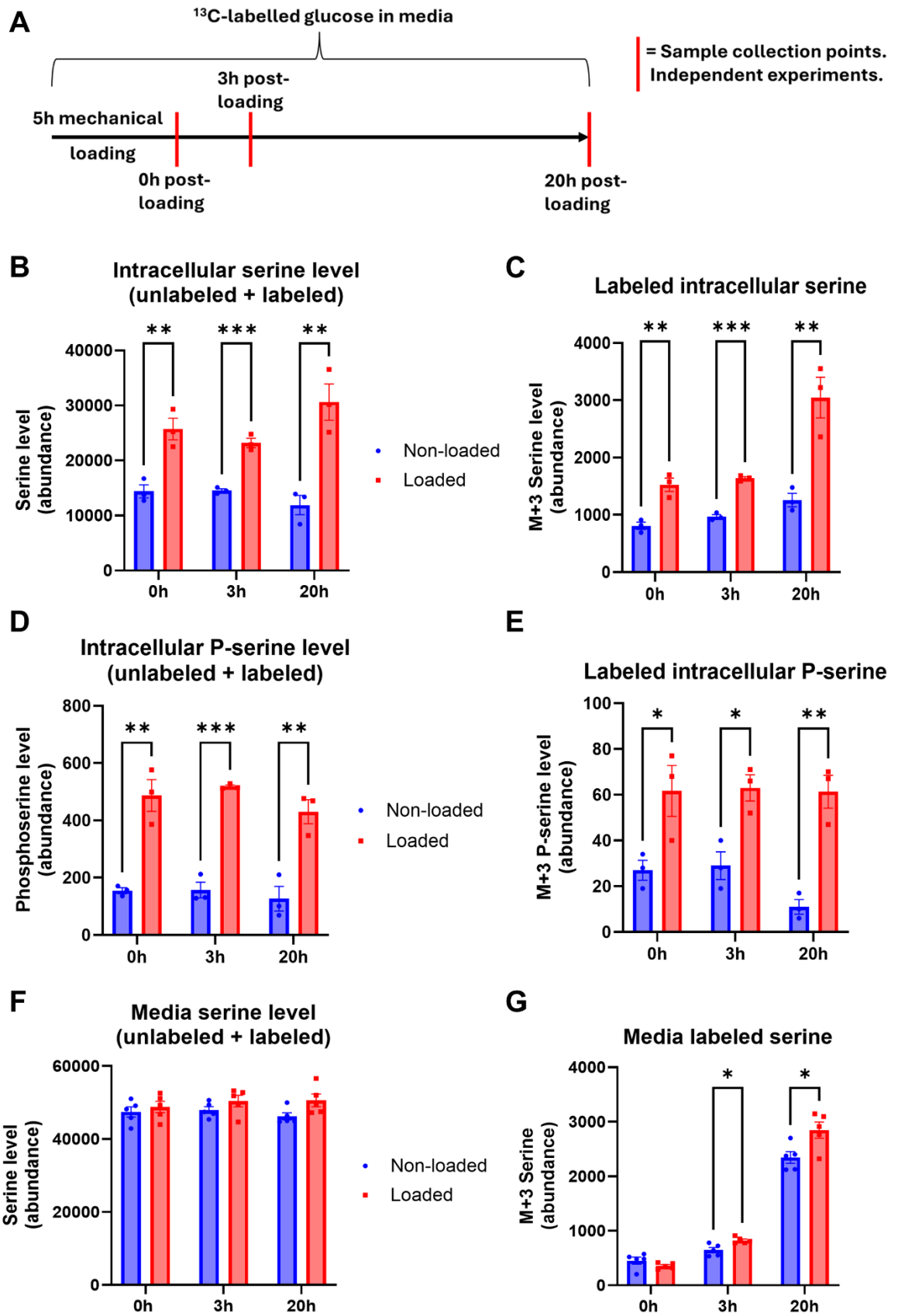

Fig. 4 Mechanical loading increased glucose-derived carbon incorporation into serine and phosphoserine in HUVECs. **A)** A schematic diagram of the time points of the ^{13}C-(U)-glucose experiment. **B)** Total intracellular serine level (unlabeled + labeled). **C)** Newly synthesized

(M+3) serine level. **D)** Total intracellular phosphoserine (P-serine) level (unlabeled + labeled). **E)** Newly synthesized (M+3) phosphoserine level. **F)** Total media (extracellular) serine level (unlabeled + labeled). **G)** Newly synthesized (M+3) media serine level. Sample sizes were n = 3 per group per time point in intracellular analyses and n = 5 in media analyses. Individual values are plotted, and data are presented as mean ± SEM. *$p < 0.05$, **$p < 0.01$, ***$p < 0.001$

Serine synthesis pathway enzyme phosphoglycerate dehydrogenase (PHGDH) is critical for endothelial cell anabolism

To assess the role of the serine synthesis pathway in HUVECs, we first inhibited the rate-limiting serine synthesis pathway enzyme PHGDH (Figure 5A) and evaluated its effects on proliferation. For this, we used two structurally distinct inhibitors, NCT-503 and CBR-5884. We discovered that both PHGDH inhibitors decreased the proliferation of HUVECs (Fig. 5B) but did not induce cell death (Figure 5C). We also tested whether the PHGDH inhibitors affect protein synthesis and glucose usage for cellular biomass production. We found that both PHGDH inhibitors decreased protein synthesis and glucose-derived carbon incorporation into proteins, RNA, and lipids (Fig. 5D-F). Next, we used a lentiviral vector to overexpress PHGDH in HUVECs (Fig. 5G). We found that the overexpression of PHGDH led to a ~10% increase in protein synthesis ($p < 0.01$, Fig. 5H) and a trend for increased proliferation ($p = 0.088$, Fig. 5I). Finally, we tested whether mechanical loading affects protein synthesis and proliferation of HUVECs. We found that mechanical loading did not affect the total protein synthesis and proliferation of HUVECs (Supplementary Fig. 8). Overall, these data suggest that the PHGDH has an important role in endothelial cell growth.

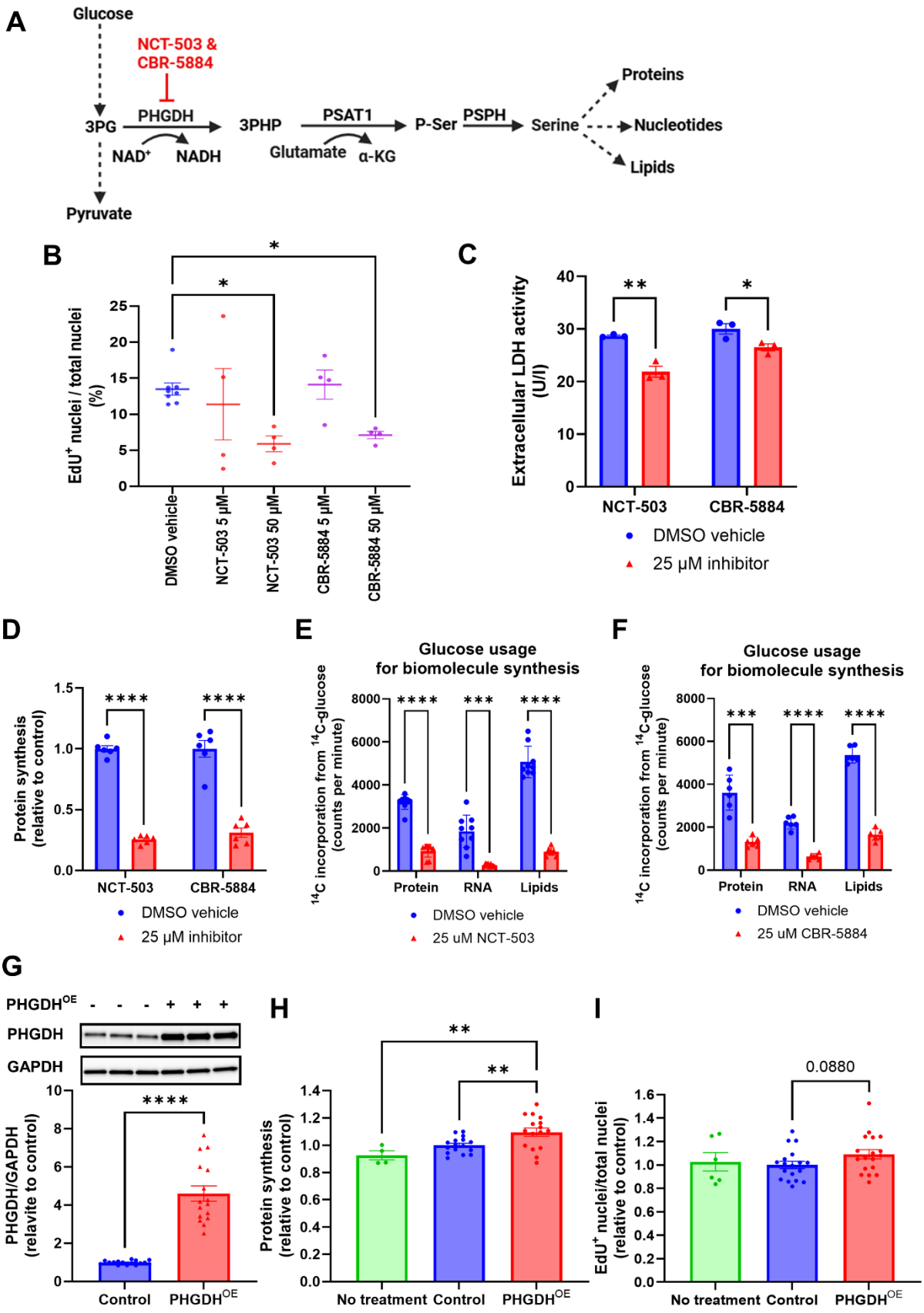

Figure 5. Effects of the serine synthesis pathway enzyme phosphoglycerate dehydrogenase (PHGDH) manipulation on cell proliferation, protein synthesis, and glucose usage for biomolecule synthesis in HUVECs. **A)** Schematic presentation of the serine synthesis

pathway. **B)** PHGDH inhibitors decreased the proliferation of HUVECs, as assessed by EdU analysis. Each group was statistically compared to the DMSO vehicle control (n = 8 in the DMSO control group and n = 4 in each inhibitor group). **C)** PHGDH inhibitors did not induce cell death according to the lactate dehydrogenase (LDH) activity measured from conditioned media as a marker of membrane damage and cell death (i.e., increased LDH activity would indicate membrane damage and cell death) (n = 3). **D)** protein synthesis (^{14}C-valine incorporation into proteins) in response to PHGDH inhibitors (n = 6). **E)** Glucose-derived carbon incorporation into proteins, RNA, and lipids in response to NCT-503 (n = 9). **F)** Glucose-derived carbon incorporation into proteins, RNA, and lipids in response to CBR-5884 (n = 6). **G)** PHGDH level in response to overexpression treatment (n = 16). **H)** Protein synthesis (^{14}C-phenylalanine incorporation into proteins) in response to PHGDH overexpression treatment (n = 16, but in no treatment group n = 4). **I)** Cell proliferation in response to PHGDH overexpression treatment (n = 24, but in no treatment group n = 6). Individual values are plotted, and data are presented as mean ± SEM. *$p < 0.05$, **$p < 0.01$, ***$p < 0.001$, **** $p < 0.0001$

Discussion

In this study, we unraveled the effects of mechanical loading on skeletal muscle and endothelial cells and identified both shared and cell type-specific responses. Notably, both muscle and endothelial cells released acetate into the media and induced gene expression changes typically seen after exercise. However, transcriptomic responses exhibited several contrasting patterns, e.g. electron transport chain (ETC) complex genes were upregulated in muscle cells but downregulated in endothelial cells. Overall, endothelial cells demonstrated more pronounced responses to mechanical loading, particularly in amino acid metabolism as well as transcriptomic pathways related to angiogenesis and growth. Furthermore, using a ^{13}C-(U)-glucose tracer, we observed that mechanical loading enhanced glucose-derived serine synthesis in endothelial cells. Overexpression of the serine synthesis enzyme PHGDH promoted protein synthesis of endothelial cells, whereas PHGDH inhibitors decreased proliferation and anabolic activity, highlighting the possible role of serine synthesis in endothelial cell growth and angiogenesis.

Both muscle and endothelial cells released acetate into the media in response to mechanical loading, which was observed with two different analysis methods. Previously, we found that electrically evoked myotube contractions also induced acetate release from murine myotubes (Lautaoja *et al*, 2021). In humans, it has been found that acetate is released into the bloodstream (van Hall *et al*, 2002) and urine (Schranner *et al*, 2020) after exercise. Moreover, serum acetate concentrations have been found to be greater in physically active individuals compared to inactive individuals (Kujala *et al*, 2013). Therefore, acetate could be a possible exerkine (i.e. a signaling molecule released in response to exercise) released by not only muscle cells but also endothelial cells. One of the most relevant functions of acetate is acting as an immunomodulator and promoter of T-cell effector function and regulating differentiation of $CD4^+$ T-cell helper cells (Jing *et al*, 2023; Miller *et al*, 2023; Qiu *et al*, 2019). This may partly explain the effects of exercise in enhancing immune system function and increasing $CD4^+$ T-helper cell count in humans (Chastin *et al*,

2021). This is particularly interesting, as factors secreted by $CD4^+$ T-cells seem to be important in angiogenesis, myogenesis, and muscle regeneration (Kwee *et al*, 2018; Schiaffino *et al*, 2017). In addition, the potential source of acetate after mechanical loading is interesting as acetate can be produced from (A) acetyl-CoA by certain acyl-CoA thioesterases (Horibata *et al*, 2013), (B) from pyruvate by ketoacid dehydrogenases and reactive oxygen species (Liu *et al*, 2018), and (C) by deacetylation of proteins (Bose *et al*, 2019). Of these, at least reactive oxygen species production is induced in muscle by exercise (Powers *et al*, 2024). Thus, acetate's possible role as an exerkine and its links to the immune system or other human physiological systems should be studied further.

Endothelial cells and muscle cells also demonstrated different, and even opposite transcriptomic responses to mechanical loading, most prominently in oxidative phosphorylation-related pathways and ETC complex genes. Oxidative phosphorylation-related genes were upregulated in muscle cells, and skeletal muscle is known to upregulate mitochondrial biogenesis and oxidative phosphorylation in response to physiological stress, such as exercise (Smith *et al*, 2023). One of the well-known mechanisms regulating these exercise adaptations is the AMPK-PGC1α pathway (Hood *et al*, 2016). In our study, although PGC1α gene expression was unchanged in muscle cells, we did observe an increase in *PPARD* expression after mechanical loading. PPARD is upstream of PGC1α (Fan & Evans, 2015) and has also been linked to enhanced oxidative metabolism in skeletal muscle (Wickramasinghe *et al*, 2022). Furthermore, muscle cells also demonstrated an upregulation of the *NR4A3* gene, which has recently been shown to be one of the most exercise-responsive genes (Pillon *et al*, 2020), and essential in glucose metabolism and anabolism, such as ribosome biogenesis in primary muscle cells (Smith *et al*, 2024). In line with the upregulation of *NR4A3*, we also observed increases in the *ribosome biogenesis* GO:BP pathway after mechanical loading. Moreover, we saw a decrease in myostatin (*MSTN*) expression after mechanical loading in muscle cells (Supplementary Table S1), which is a common response after a single bout of resistance exercise (Hulmi *et al*, 2007; Kim *et al*, 2005). These results demonstrate that mechanical loading of human skeletal muscle cells recapitulates several of the common effects of exercise seen *in vivo*.

In endothelial cells, transcriptomic results showed that mechanical loading induced upregulation of genes related to endothelial cell development, RNA splicing, and negative regulation of catabolic processes, and moreover, downregulation of cellular senescence-related genes. Many of the endothelial cell development genes were also found to increase in response to acute aerobic exercise in human skeletal muscle tissue, which is known to be highly vascularized (Englund *et al*, 2021; Pepe & Albrecht, 2023; Pillon *et al*, 2020). Furthermore, our results showed upregulation of mechanosensitive genes commonly associated with an atheroprotective endothelial phenotype, which are typically induced by flow-mediated mechanical stress (Li *et al*, 2024; Davis *et al*, 2023; Peng *et al*, 2019). Our findings point out that a similar effect was seen after cyclic stretching, which is comparable to skeletal muscle movement. We also found that genes related to VEGF response, including VEGF receptors 1 & 2 (*FLT1 & KDR*), were upregulated in endothelial cells. Related to these, *VEGFA*

expression was also increased in mechanically loaded muscle cells, and it has been hypothesized that skeletal muscle stem cells recruit ECs via VEGFA expression and this interaction is important for muscle stem cell self-renewal (Verma *et al*, 2018). In addition, similar cyclic stretch as used in this study, has previously been shown to enhance endothelial cell proliferation (Li & Sumpio, 2005) and angiogenesis (Yung *et al*, 2009). Mechanical loading also induced upregulation of insulin receptor signaling pathways in endothelial cells, and more specifically, these pathways included genes such as *FGF5*, *PDPK1,* and *KRAS* which were upregulated in both endothelial cell lines. *FGF5* has previously been shown to promote angiogenesis (Seo *et al*, 2016), and *PDPK1* and *KRAS* are linked to the PI3K/Akt signaling pathway (Manning & Toker, 2017), which is known to regulate angiogenesis and endothelial cell growth (Kobialka & Graupera, 2019). Since exercise-induced angiogenesis is a well-known and documented physiological phenomenon in humans (Ross *et al*, 2023), our results suggest that, similarly to muscle cells, mechanical loading of endothelial cells also recapitulates the effects of exercise *in vivo*.

We found intriguing that the oxidative phosphorylation pathways and ETC complex genes were coordinately downregulated in endothelial cells, which was completely opposite to the response in muscle cells. It has previously been shown that endothelial cells primarily rely on glycolysis for ATP production despite having access to oxygen, and that vessel sprouting of endothelial cells *in vitro* is regulated by glycolysis (De Bock *et al*, 2013). It is also known that proliferating cells similarly rely on glycolysis to ensure adequate availability of metabolic intermediates for cell growth, which is described as the Warburg effect (Lunt & Vander Heiden, 2011). In the Warburg effect, glycolytic intermediates are used to produce e.g., nucleotides, serine, alanine, glycine, and cysteine needed for growth. Thus, the transcriptomic results collectively suggest a possible link between a metabolic shift towards glycolytic ATP production and increased growth in mechanically loaded endothelial cells.

In line with the transcriptomic results, the metabolite enrichment analysis showed that the Warburg effect was the third most enriched pathway in endothelial cells. Moreover, ^{13}C-glucose tracing analysis revealed that the abundance and synthesis of growth-related amino acids: serine, phosphoserine, and alanine increased after mechanical loading at multiple time points in endothelial cells. In the serine synthesis pathway, PHGDH is an essential enzyme for serine production and anabolism in many different cell types (Handzlik & Metallo, 2023; Mäntyselkä *et al*, 2024; Stegen *et al*, 2022). Our further experiments revealed that overexpression of PHGDH in endothelial cells increased protein synthesis, while commonly used non-competitive PHGDH inhibitors decreased proliferation, protein synthesis, and glucose-derived carbon incorporation into proteins, RNA, and lipids. This is similar to what we recently demonstrated in muscle cells (Mäntyselkä *et al*, 2024). Loss of PHGDH has previously been shown to cause lethal defects in angiogenesis in mice, and knockdown of PHGDH impairs EC proliferation (Vandekeere *et al*, 2018). Moreover, PHGDH knockdown impairs heme synthesis while PHGDH overexpression increases endothelial spheroid sprouting in cultured endothelial cells (Vandekeere *et al*, 2018). Interestingly, in this current study, we also observed upregulation of heme

signaling- and sprouting angiogenesis-related genes in response to mechanical loading. These results indicate that mechanical stimuli and PHGDH overexpression similarly affect endothelial cells to support their function, possibly via increased serine production. The serine synthesis pathway has also been identified as a major upregulated metabolic pathway in tumor endothelial cells, and the loss of PHGDH reduced tumor vasculature (Zhang *et al*, 2023). Therefore, our results and the existing evidence highlight that the serine synthesis pathway, especially PHGDH, is crucial for endothelial cell function and anabolism. Further studies are needed to investigate the importance of the serine synthesis pathway and PHGDH in endothelial cells after exercise or exercise-mimicking stimuli.

The mechanism of how mechanical loading activates serine synthesis in endothelial cells was not studied here. However, the mechanical loading did not increase the serine synthesis pathway gene expression, indicating that the increased serine synthesis is regulated by other mechanisms. Recently, it was found that epithelial cadherin (E-cadherin) induces serine synthesis in cancer cells (Lee *et al*, 2024) and others also found that shear stress (another form of mechanical loading) increases glucose uptake in endothelial cells through the activation of vascular endothelial cadherin (VE-cadherin) (Cronin *et al*, 2024). VE-cadherin and proteins linked to it are important for mechanotransduction in endothelial cells (Kong *et al*, 2022; Nan *et al*, 2023). Here, we found increased expression of genes encoding proteins linked with VE-cadherin. In further studies, the possible mechanism for the activation of serine synthesis through VE-cadherin, or other upstream regulators, should be examined.

Strengths and limitations

We used two different human endothelial cell types and primary human skeletal muscle cells. The loading induced several common exercise-induced and mechanosensitive genes, suggesting an external validity of the model. Moreover, several of the transcriptomic responses to mechanical loading were similar between the two endothelial cell types (HUVEC and HCMEC), suggesting that many of the changes can be applied to endothelial cells in general. We also replicated the main metabolite results with different methods. For example, acetate release was observed with both ^{1}H NMR spectroscopy and UHPLC-MS. In addition, the increased serine, alanine, and proline content and synthesis were detected by targeted metabolomics and isotopic tracing from multiple time points. We also conducted mechanistic experiments to focus on the main findings regarding increased serine and growth-directed gene expression revealed by the -*omics* analyses.

The study also has limitations. We conducted the experiments with monolayers of cells (i.e., two-dimensionally), and therefore, myotubes were not aligned unidirectionally while the mechanical loading was unidirectional. In contrast, smaller endothelial cells could change their alignment against the direction of stretch. This difference in the ability to change alignment may in part explain why we detected fewer molecular changes in myotubes compared to endothelial cells. Overall, the data suggest that the mechanical loading model for two-dimensionally cultured cells is suitable for endothelial cells, which grow in monolayers, also *in vivo*, while

myotubes may need to be loaded three-dimensionally to sufficiently mimic exercise in future studies.

Conclusion

Mechanical loading induces common and cell type-specific transcriptomic and metabolomic responses in endothelial and skeletal muscle cells. In general, several of the effects recapitulated what is observed *in vivo* after exercise. Both endothelial and muscle cells released acetate in response to mechanical loading, and therefore acetate's potential role as an exerkine should be studied in the future. The responses to mechanical loading were larger in endothelial cells, revealing increased serine synthesis as one of the main metabolic changes. These results, together with mechanistic experiments, highlight that mechanical stimulus, serine synthesis, and PHGDH are interconnected and may be important for endothelial cell growth and development. The potential importance of the mechanical loading and serine synthesis pathway for improved vascularization should be studied *in vivo* in further studies.

Materials and methods

Endothelial and muscle cells

We used human umbilical vein endothelial cells (HUVEC, Cat# C-12200, PromoCell), human cardiac microvascular endothelial cells (HCMEC, Cat# C-12285, PromoCell), and primary human skeletal muscle (HSkM) cells. The latter were obtained as previously (Mäntyselkä *et al*, 2024) from two healthy 25-34-year-old volunteers (1 male and 1 female). Vastus lateralis muscle biopsies were obtained under local anesthesia with the Bergström biopsy needle. The human study (Halonen *et al*, 2024) was conducted in accordance with the Declaration of Helsinki and was approved as part of a larger study by the Ethics Committee of the University of Jyväskylä (857/13.00.04.00/2021). All participants gave their written informed consent for inclusion before they participated in the study.

Cell culture

The HUVEC and HCMEC cells were cultured in endothelial cell growth medium (EGM) (Cat# C-22010, PromoCell) supplemented with EGM SupplementMix (Cat# C-39215, PromoCell) and 1% (vol/vol) of 1000 U/ml penicillin-streptomycin (P/S, Cat# 11548876, Gibco). HSkM cells were cultured in growth medium (GM) consisting of high glucose (4.5 g/l) Dulbecco's Modified Eagle Medium (DMEM, Cat# 10313021, Gibco) supplemented with 20% (vol/vol) fetal bovine serum (FBS, Cat# 10270106, Gibco), 1% (vol/vol) of 1000 U/ml P/S and 1% (vol/vol) 200 mM L-glutamine (Cat# 11500626, Gibco).

After reaching over 80% confluency in culture flasks, the cells were seeded (~20,000 cells/cm^2) on polydimethylsiloxane (PDMS) chambers (Cat# STB-CH-04, STREX). PDMS chambers were pre-coated with FBS for 24 h and with 0.2% gelatin for an

additional 24 h. The PDMS chambers were placed in 150 mm diameter Petri dishes, two chambers per dish. Cells were grown on PDMS chambers until reaching over 80% confluency. After that, HUVEC and HCMEC cells were mechanically loaded, as described in the next section. In the case of HSkM cells, at 80% confluency the GM was replaced with differentiation medium (DM) containing high glucose DMEM, 2% (vol/vol) horse serum (HS, Cat# 26050088, Thermo Fisher Scientific), 1% P/S, 1% L-glutamine and 1% (vol/vol) Insulin-Transferrin-Selenium-X supplement (ITS-X, Cat# 51500056, Gibco). To induce myoblast fusion into myotubes, the cells were cultured in DM for 4-5 days and DM was changed every 48 h. Cells were cultured at 37 ℃ in a 5% CO_2 atmosphere all the time.

Mechanical loading set-up

Mechanical loading of cultured cells was achieved with a commercial cell culture pacing system (C-Pace EM 100, IonOptix) paired with a motor-powered mechanical stimulation unit (C-Stretch 100, IonOptix). The C-Stretch mechanical stimulation unit consists of a motor-driven tray that causes uniaxial elongation of the PDMS chambers inserted in the device and exposes cells, that are attached to the bottom of the chamber, to mechanical load.

As mentioned, cells were seeded onto 12 PDMS chambers for each stretch experiment, with 6 chambers loaded into the C-Stretch unit in series, and 6 chambers left as static controls. The stretch unit was thoroughly cleaned with 70% EtOH before use. Fresh media was changed for all chambers prior to starting the experiment. The stretch unit was then placed in an incubator with conditions of 37 ℃ and 5% CO_2 atmosphere along with the 6 control chambers. A cyclic mechanical stretch with a frequency of 1 Hz and 12% elongation was applied for 5 h. For each one-second cycle, a trapezoidal waveform of 0.4 s stretch, 0.1 s hold, 0.4 s return, and 0.1 s hold, was used to keep the velocity of the deformation of the silicone chamber at a moderate speed.

Lactate dehydrogenase activity assay

Lactate dehydrogenase activity (LDH) was measured from conditioned media as an indicator of possible membrane damage and cell death (Legrand *et al*, 1992). The analysis was performed as previously (Mäntyselkä *et al*, 2024) using an LDH Activity Assay Kit (Cat# 981906, Thermo Fisher Scientific).

RNA extraction and analyses

RNA isolation, library preparation and sequencing

RNA was extracted using a commercial column-based RNA isolation kit (NucleoSpin® RNA, Cat# 740955.250, Macherey-Nagel) immediately after the 5-hour mechanical loading. The PDMS chambers were washed with PBS, and cells were lysed by pipetting back and forth vigorously with lysis solution (350 µl of guanidium thiocyanate lysis buffer + 3.5 µl of β-mercaptoethanol). Extraction was then continued according to the kit's instructions. An additional centrifugation step of 30 s at 11 000 g was included at the end to ensure complete removal of the wash buffer. Bound RNA was then eluted into a volume of 60 µl of RNase-free water. The

collected elution was then aliquoted and samples were immediately transferred to -80 °C. RNA quality control, library preparation and sample sequencing were performed at Novogene (Cambridge, United Kingdom), utilizing an Illumina NovaSeq 6000 platform, producing 150bp paired-end reads. Filtering of raw sequence data was also conducted by Novogene in the following way: (1) removing reads containing adapters, (2) removing reads containing >10% of unsolvable bases and (3) removing reads containing >50% of low quality bases (Qphred ≤ 5). Filtered RNA sequencing data is available in the Gene Expression Omnibus (GEO) data repository (accession number: GSE288064).

Read alignment, normalization and filtering

Reads were aligned to the human genome (build GRCh38.95) using the Bowtie2 software (Langmead & Salzberg, 2012), with alignment rates >80% for all the samples. The aligned and mapped reads were later annotated and quantified using the Rsubread package in R/Bioconductor software (Liao *et al*, 2014), with the human GRCh38.110 genome build as annotation reference. The obtained gene counts were transformed to counts-per-million (CPM) using the edgeR package in the R/Bioconductor software (Robinson *et al*, 2010). Genes with a CPM < 1 in three samples or more in each group (50%), were subsequently filtered out as described in (Chen *et al*, 2016). The resulting expression data were finally normalized using the trimmed mean of M-values (TMM) algorithm (Robinson & Oshlack, 2010).

Differential gene expression and pathway analyses

Differential gene expression (DGE) analyses were implemented through the R/Bioconductor limma-voom pipeline (Ritchie *et al*, 2015). The voom-function of the limma package was initially executed to format the data appropriately (Law *et al*, 2014), after which empirical Bayesian statistics were computed to rank genes based on their evidence for differential expression. To account for type I errors induced by multiple testing, the Benjamini-Hochberg method was used to adjust the tests' *p*-values, retrieving an adjusted *p*-value (adj. *p*). Genes with a $\log_2$FC ≥ 0.5 and adj. *p* ≤ 0.05 were regarded as differentially expressed. For subsequent Gene Set Enrichment Analysis (GSEA) genes were ranked in an unbiased way by multiplying the $\log_2$FC by the -log10 of the adj. *p* to consider both the magnitude and consistency of the change in gene expression. GSEA was performed with the clusterProfiler R-package (Yu *et al*, 2012) with Gene Ontology: Biological Process (GO:BP), Reactome, and the Kyoto Encyclopedia of Genes and Genomes (KEGG) serving as reference databases. Ontologies and pathways were considered significantly enriched if their corresponding tests yielded an adj. p-value <0.05. In addition, gene set overrepresentation analysis (ORA) of the significantly up- or downregulated genes ($\log_2$FC ≥ 0.5 & adj. *p* ≤ 0.05) was conducted using the ShinyGO web-application v0.81 (https://bioinformatics.sdstate.edu/go/) (Ge *et al*, 2020) from GO:BP pathways. Pathway minimum size was set to 2 and maximum to 5000 and the FDR cutoff for significant pathway enrichment was set to 0.05. All analyses implemented in R/Bioconductor included the core software version 4.3.1 with the R-studio interface version 2024.04.2.

Meta-analysis of skeletal muscle response to exercise (MetaMEx)

We examined gene expression of the *Endothelial cell development* pathway (GO:0001885, 72 genes, list checked on 10.06.2025) in response to acute aerobic exercise using the MetaMEx browser-based tool (https://www.metamex.eu/app/metamex) (Pillon *et al*, 2020). All the other settings were kept as a default, except that only the healthy population was included.

Metabolite extraction and analyses

^{1}H NMR spectroscopy metabolomics

Metabolites from the media samples were extracted as previously (Mäntyselkä *et al*, 2024; Lautaoja *et al*, 2021). Cell-free medium samples were also included as a reference to assess the uptake and release of metabolites. Dried samples were reconstituted with 200 µL of sodium phosphate buffer (150 mM, pH = 7.4) in 99.8% deuterium oxide (Acros Organic; Thermo Fisher Scientific) containing 0.5 mM 3-(trimethylsilyl)propanesulfonic-d_6 acid sodium salt (DSS-d_6; IS-2 Internal Standard, Chenomx Inc.) and transferred to round-bottom 3-mm OD NMR tubes (Cat# 341-PP-7, Wilmad). Data collection was carried out at 25 °C using the Bruker AVANCE III HD NMR spectrometer, operating at 800 MHz ^{1}H frequency equipped with a cryogenically cooled ^{1}H, ^{13}C, ^{15}N triple-resonance probe head (Bruker Corporation). The ^{1}H nuclear magnetic resonance (^{1}H NMR) spectra were collected as previously (Lautaoja *et al*, 2021). ^{1}H NMR spectra were processed, and metabolites were identified and quantified with the Chenomx 10.0 software (Chenomx).

UHPLC-MS/MS targeted metabolomics

Intracellular metabolites were collected and extracted as previously (Mäntyselkä *et al*, 2024) with minor modifications. In brief, 200 µL of ice-cold 80% methanol was added to each stretching chamber, and metabolites from three chambers were pooled for one sample. Dried samples were reconstituted with 40 µl of 50-50 acetonitrile-water mixture (vol/vol) before analysis. Metabolites were analyzed as previously (Mäntyselkä *et al*, 2024). Briefly, metabolites were separated with an Atlantis Premier BEH Z-HILIC UHPLC column (1.7 µm, 2.1 x 100 mm) which was used with an Agilent 1290 Infinity ultra-high-performance liquid chromatography (UHPLC) system. *Mobile phase A* was 15 mM ammonium bicarbonate (pH = 9.0) in water, and *mobile phase B* was 15 mM ammonium bicarbonate (pH = 9.0) in 90% acetonitrile-10% water. The flow rate was 0.7 mL/min, the column oven temperature was 40 °C, and the injection volume was 3 µl. The following gradient elution was used: the initial concentration of 90% *B* was held for 1 min and then was linearly decreased to 65% *B* over the next 5 min and was held for 1 min at 65% *B*. Then *B*% was increased to 90% over the next 1 min and was held 2 min at 90% *B* before next injection. The UHPLC system was coupled with an Agilent 6460 triple quadrupole mass spectrometer operated with dynamic multiple reaction monitoring mode (dMRM) as previously described (Mäntyselkä *et al*, 2024). A mixture of target metabolites (concentrations between 10 and 50 µM) was injected eight times at the

beginning of the analysis and after every 6-8 samples for quality control and metabolite identification purposes.

Acetate was analyzed from media samples using the above-described chromatographic method and the UHPLC-MS instrument which was operated on negative polarization. For acetate, selected ion monitoring (e.g., pseudo-MRM (Qasem *et al*, 2017)) of *m/z* 59 was done. The following parameters were used for the selected ion monitoring experiment: fragmentor: 80; collision energy: 1; cell accelerator voltage: 4. The other ion source parameters were the same as previously reported (Mäntyselkä *et al*, 2024). Retention time and linearity of the signal were tested with 10, 20, 40, 80, and 160 µM acetate standards that were prepared using sodium acetate (Cat# 106268, Merck). The acetate standard was also used for a spike-in experiment.

Batch correction, normalization, and statistical analyses of metabolomics data

Targeted UHPLC-MS/MS data and ^{1}H NMR data were measured within two batches and therefore they were batch effect corrected using the EigenMS method on the MetaboAnalyst 6.0 platform (https://www.metaboanalyst.ca/). In the case of UHPLC-MS/MS, data collected with negative and positive modes were separately batch-corrected before combining the data. Single missing values within different groups were replaced with 1/5 of the minimum detected values. Metabolite concentrations/abundances were $\log_2$ transformed for statistical testing with the Student's t-test with significance set at $p < 0.05$ and fold change > I1.1I.

Metabolite overrepresentation analysis

MetaboAnalyst 6.0 platform was used for the metabolite overrepresentation analysis. Names of the significantly altered metabolites were uploaded. Default settings were used (SMPDB pathway and '*Only use metabolites sets containing at least 2 entries*' option were used).

^{13}C-glucose labeling experiments and analyses

Glucose-free and phenol red-free endothelial cell medium (Cat# H1168GPF, Cell Biologics) medium including medium kit's supplements was supplemented with 5.5 mM U-$^{13}C_6$-D-glucose (Cat# CLM-1396-1, Cambridge Isotope laboratories, isotopic purity 99%). This medium was changed to the cells just before the initiation of the experiment. Intracellular metabolites were extracted with the same protocol as for targeted UHPLC-MS/MS metabolomics, but this time two chambers were pooled instead of three. Media metabolites were extracted with the same protocol as for ^{1}H NMR metabolomics described above except now 100 µl of media from each chamber was mixed with 200 µl of methanol. Intracellular and medium metabolites were reconstituted into 45 µl and 400 µl of 50-50 acetonitrile-water solution, respectively. Pooled quality control (QC) samples were prepared by transferring a small aliquot of each sample into a vial (separate QC samples for intracellular and medium metabolites). Selected amino acids were analyzed with the same method as in targeted UHPLC-MS/MS metabolomics described above but the MRM transitions were modified (Supplementary Table S7) allowing analysis of the isotopomers of the

selected amino acids. The data was processed and integrated with MRMPROBS_v.3.66 software (Tsugawa *et al*, 2014). Phosphoserine and glycine were processed and integrated with Agilent Qualitative Navigator B.08.00 software because of their lower abundance. Isotope natural abundances were corrected with IsoCor 2.2.2 software (Millard *et al*, 2019) as earlier reported (Yoon *et al*, 2023).

Chemical inhibitors

For chemical inhibitor experiments, two different PHGDH inhibitors NCT-503, (Cat# HY-101966) and CBR-5884 (Cat# HY-100012) were obtained from MedChemExpress. Inhibitor stock solutions were prepared in DMSO, and the DMSO was also used as vehicle control. The inhibitors were used in concentrations of 5, 25, and 50 µM as previously have been used for different cell types (Mäntyselkä *et al*, 2024; Zhang *et al*, 2018; Białopiotrowicz *et al*, 2020; Zhang *et al*, 2022). The exact inhibitor concentration for each experiment is stated in the legends or caption of Fig. 5. Further details of inhibitor experiments are described in the next two sections.

Cell proliferation analysis with EdU labeling

Effects of chemical inhibitors (see the section above) on cell division capacity were evaluated using a Click-iT EdU imaging kit (Cat# C10338, Invitrogen). HUVEC cells were plated onto a 96-well plate in Endothelial cell GM and let to grow in subconfluent culture for 24 h. Exposures were added to the wells, four parallel wells for each condition, and eight parallel for the control condition (DMSO vehicle). After 20 h incubation of exposures, 5-ethynyl-20-deoxyuridine (EdU) was added for 4 h. Cells were fixed with 4% PFA for 15 min, washed with 3% bovine serum albumin (BSA) in PBS, and permeabilized with 0.5% Triton X-100 in PBS for 20 min RT, and the Click reaction was done according to the manufacturer's instructions. Before imaging, DAPI (0.5 µg/ml) was added to visualize all nuclei. Cells were imaged using a Nikon A1R confocal microscope. The microscope was automated to find optimal focus in each well, image every well, and take 2-9 views per well so that at least 300 nuclei were imaged. Detected nuclei (all nuclei + EdU stained nuclei) were analyzed using an in-house built Fiji script (https://github.com/seiryoku-zenyo/simple_ratio_DAPIvsPositive-nuclei/tree/main). Shortly, image data was segmented using a deep learning algorithm, separately for DAPI-positive nuclei and EdU-positive nuclei. Next, the ratio between DAPI and EdU nuclei was counted. The data is presented as a fraction (%) of EdU-positive nuclei out of total (DAPI) nuclei.

Click-iT EdU imaging kit (Cat# C10339, Invitrogen) was also used to determine the effect of PHGDH overexpression on HUVEC proliferation. Cells were cultured on 13 mm diameter coverslips (10 000 cell/cm^2) coated with 0.2% gelatin for 24 h after which cells were incubated with EdU labeling solution for 5 h. Cells were fixed, washed, and permeabilized as above. Click reaction buffer was prepared as described by the manufacturer, added to the cells, and incubated for 30 min protected from light. DAPI (0.5 µg/ml) was used to detect all the nuclei. Cells were imaged with a confocal microscope (Zeiss LSM700) and the number of stained nuclei was calculated with Fiji manually. The data is presented as a fraction (%) of EdU-positive nuclei out of total (DAPI) nuclei.

To assess the effects of mechanical loading on HUVEC proliferation, cells were mechanically loaded as described earlier, detached, and plated on 13 mm diameter coverslips as above. The EdU analysis was performed as above.

Carbon-14 labeling

The following radioisotope tracers were used: ^{14}C-[U]-glucose (0.2 mCi/mL, Cat# NEC042V250UC, PerkinElmer); ^{14}C-[U]-L-valine (271.0 µCi/mmol, Cat# NEC291EU050UC, PerkinElmer); and ^{14}C-[1]-L-phenylalanine (0.1 mCi/mL, Cat# NEC859S050UC, PerkinElmer). Only one tracer per experiment was used, and the dilution of the tracers was 1 µL/mL (vol/vol) in the culture media. Two milliliters of culture media were used per well of a 6-well plate, and one milliliter per stretching chamber

HUVECs for PHGDH inhibitor experiments were seeded onto 0.2% gelatin-coated 6-well plates at a density of 12,500 cells/cm². The cell population was expanded for 2 days, and the inhibition experiments were initiated by changing the media to experimental media containing 25 µM of inhibitor and a radioisotope tracer. After incubating cells for 48 h with inhibitor and tracer, proteins, RNA, and lipids were extracted, and liquid scintillation counting was conducted as previously (Mäntyselkä *et al*, 2024). When protein synthesis was measured during and after mechanical loading, tracer was added to the medium just before the initiation of the 5 h mechanical loading. After the loading, HUVECs were incubated for an additional 20 h in the medium, and then proteins were extracted.

PHGDH overexpression

The PHGDH overexpression construct pLJM5-WT PHGDH was a gift from David Sabatini (Addgene plasmid #83901; http://n2t.net/addgene:83901; RRID: Addgene_83901) (Pacold *et al*, 2016). Lentivirus particles were prepared and distributed by Biomedicum Virus Core facility supported by HiLIFE and the Faculty of Medicine, University of Helsinki, and Biocenter Finland. The control construct, clone SHC002 (Scrambled shRNA in pLKO.1) was from Sigma Aldrich MISSION shRNA library, distributed by Genome Biology Unit core facility supported by HiLIFE and the Faculty of Medicine, University of Helsinki, and Biocenter Finland. The Biomedicum Virus Core facility also determined the p24 capsid protein concentration with an enzyme-linked immunosorbent assay (ELISA). p24 concentrations were used to calculate the number of virus particles needed for transduction (1 pg of p24 = 100 transducing units).

HUVECs were cultured in T75 flasks. After reaching 50% confluence, 10 ml of medium containing lentiviruses (MOI = 50) and polybrene (5 µg/ml), was added to the cells. Polybrene (Cat# TR-1003, Sigma-Aldrich) was used to improve infection efficiency. HUVECs were incubated with lentiviruses for 24 hours. After transduction, the cells were resuspended in a fresh endothelial cell medium, cultured overnight, and used for further experiments. HUVECs expressing scrambled shRNA and HUVECs without virus treatment were used as controls for the PHGDH overexpression construct.

Protein extraction and Western Blotting

HUVECs expressing either the PHGDH overexpression system or shControl gene were cultured in 6-well plates (5000 cells/cm^2) in endothelial cell medium supplemented with 1 µl/ml (vol/vol) ^{14}C-[1]-L-phenylalanine (43 mCi/mmol, Cat# NEC859S050UC, PerkinElmer). After 48 hours, cells were homogenized in lysis buffer containing 20 mM HEPES (pH 7.4), 1 mM EDTA, 5 mM EGTA, 10 mM $MgCl_2$, 100 mM β-glycerophosphate, 1 mM Na_3VO_4, 1 mM DTT, 1% TritonX-100 and supplemented with protease and phosphatase inhibitors (Cat# 78442, Thermo Fisher Scientific). Cell lysates were centrifuged for 5 min at 13 000 x g, 4 ℃, and the supernatant was collected. Separate aliquots of the supernatants were used for western blotting and analysis of ^{14}C-[1]-L-phenylalanine incorporation into proteins with liquid scintillation counting (see the Carbon-14 labeling -section). Western blot analysis of PHGDH was conducted by using low-fluorescence PVDF membranes and anti-PHGDH antibody (1:5000 dilution, Cat# HPA021241, Sigma-Aldrich) as previously (Mäntyselkä *et al*, 2024) with GAPDH (1:10 000 dilution, Cat# ab9485, Abcam) as a loading control.

Statistical testing in non-*omics* analyses

Statistical tests were conducted using GraphPad Prism10.3.1 (Dotmatics). The Student's t-test was used when two groups were compared whereas one-way ANOVA with Fisher's least significant difference test was used when a control group was compared to various treatment groups. Group difference was considered statistically significant with the $p \leq 0.05$.

Acknowledgments

We thank Associate Professor Thomas M. O'Connell for valuable advice regarding ^{13}C isotopic tracing and for providing the R script for ranking the significantly altered genes. We also thank all the laboratory technicians who helped us during this study. Figures 1A, 3A, the schematic part of 5A, and the graphical abstract were created with https://www.biorender.com/.

CRediT authorship contribution statement

Sakari Mäntyselkä: Conceptualization, Methodology, Validation, Formal analysis, Investigation, Resources, Writing – Original Draft, Writing – Review & Editing, Visualization. **Erik Niemi**: Conceptualization, Methodology, Validation, Formal analysis, Investigation, Data Curation, Writing – Original Draft, Writing – Review & Editing, Visualization. **Laura Ylä-Outinen:** Conceptualization, Methodology, Investigation, Writing – Review & Editing**. Kalle Kolari:** Investigation, Writing – Review & Editing. **Liina Uusitalo-Kylmälä:** Formal analysis, Investigation, Writing – Review & Editing, Visualization. **Alfredo Ortega-Alonso:** Formal Analysis, Data Curation, Writing – Review & Editing. **Roosa-Maria Liimatainen:** Validation, Investigation, Review of the manuscript. **Vasco Fachada:** Software, Writing –

Review & Editing. **Perttu Permi:** Investigation, Writing – Review & Editing. **Elina Kalenius:** Methodology, Writing – Review & Editing, Supervision. **Juha J Hulmi:** Conceptualization, Resources, Writing – Original Draft, Writing – Review & Editing, Supervision, Project administration. **Riikka Kivelä:** Conceptualization, Resources, Writing – Original Draft, Writing – Review & Editing, Supervision, Project administration, Funding acquisition.

Funding

This work was supported by the Research Council of Finland (R.K., Grant number: 348636), the Sigrid Jusélius Foundation (R.K.), the Finnish Foundation for Cardiovascular Research (R.K., L. U-K.), the Emil Aaltonen Foundation (S.M., E.N.), and the Finnish Cultural Foundation (K.K. and J.J.H).

Disclosure and competing interest statement

The authors declare that they have no known competing financial interests or personal relationships that could have appeared to influence the work reported in this paper.

Supplementary Data

A PDF file containing the Supplementary Figures 1-8.

Excel spreadsheets:

- Table S1: List of DEGs
- Table S2: Overlapping DEGs
- Table S3: GSEA results
- Table S4: Overlapping GSEA pathways
- Table S5: Metabolomics data
- Table S6: ^{13}C-(U)-glucose labeling data
- Table S7: MRM-transitions used in ^{13}C-(U)-glucose tracing

Data availability

Filtered non-aligned RNA sequencing data and non-normalized quantified reads are available in the Gene Expression Omnibus (GEO) data repository (accession number: GSE288064). Processed transcriptomics data are shared as Supplementary Excel spreadsheets. Numerical metabolomics and isotopic tracing data are shared as Supplementary Excel spreadsheets.

References

Białopiotrowicz E, Noyszewska-Kania M, Kachamakova-Trojanowska N, Łoboda A, Cybulska M, Grochowska A, Kopczyński M, Mikula M, Prochorec-Sobieszek M, Firczuk M, *et al* (2020) Serine Biosynthesis Pathway Supports MYC-miR-494-EZH2 Feed-Forward Circuit Necessary to Maintain Metabolic and Epigenetic Reprogramming of Burkitt Lymphoma Cells. *Cancers* 12: 580

Biernat K, Kuciel N, Mazurek J & Hap K (2024) Is It Possible to Train the Endothelium?-A Narrative Literature Review. *Life Basel Switz* 14: 616

Bose S, Ramesh V & Locasale JW (2019) Acetate Metabolism in Physiology, Cancer, and Beyond. *Trends Cell Biol* 29: 695–703

Chastin SFM, Abaraogu U, Bourgois JG, Dall PM, Darnborough J, Duncan E, Dumortier J, Pavón DJ, McParland J, Roberts NJ, *et al* (2021) Effects of Regular Physical Activity on the Immune System, Vaccination and Risk of Community-Acquired Infectious Disease in the General Population: Systematic Review and Meta-Analysis. *Sports Med Auckl NZ* 51: 1673–1686

Chen Y, Lun ATL & Smyth GK (2016) From reads to genes to pathways: differential expression analysis of RNA-Seq experiments using Rsubread and the edgeR quasi-likelihood pipeline. *F1000Research* 5: 1438

Cronin NM, Dawson LW & DeMali KA (2024) Shear stress-stimulated AMPK couples endothelial cell mechanics, metabolism and vasodilation. *J Cell Sci* 137: jcs262232

Davis MJ, Earley S, Li Y-S & Chien S (2023) Vascular mechanotransduction. *Physiol Rev* 103: 1247–1421

De Bock K, Georgiadou M, Schoors S, Kuchnio A, Wong BW, Cantelmo AR, Quaegebeur A, Ghesquière B, Cauwenberghs S, Eelen G, *et al* (2013) Role of PFKFB3-driven glycolysis in vessel sprouting. *Cell* 154: 651–663

Englund DA, Zhang X, Aversa Z & LeBrasseur NK (2021) Skeletal muscle aging, cellular senescence, and senotherapeutics: Current knowledge and future directions. *Mech Ageing Dev* 200: 111595

Fan W & Evans R (2015) PPARs and ERRs: molecular mediators of mitochondrial metabolism. *Curr Opin Cell Biol* 33: 49–54

Ge SX, Jung D & Yao R (2020) ShinyGO: a graphical gene-set enrichment tool for animals and plants. *Bioinforma Oxf Engl* 36: 2628–2629

Große-Segerath L, Follert P, Behnke K, Ettich J, Buschmann T, Kirschner P, Hartwig S, Lehr S, Korf-Klingebiel M, Eberhard D, *et al* (2024) Identification of myeloid-derived growth factor as a mechanically-induced, growth-promoting angiocrine signal for human hepatocytes. *Nat Commun* 15: 1076

van Hall G, Sacchetti M & Rådegran G (2002) Whole body and leg acetate kinetics at rest, during exercise and recovery in humans. *J Physiol* 542: 263–272

Halonen EJ, Gabriel I, Kelahaara MM, Ahtiainen JP & Hulmi JJ (2024) Does Taking a Break Matter-Adaptations in Muscle Strength and Size Between Continuous and Periodic Resistance Training. *Scand J Med Sci Sports* 34: e14739

Handzlik MK & Metallo CM (2023) Sources and Sinks of Serine in Nutrition, Health, and Disease. *Annu Rev Nutr* 43: 123–151

Hinkle ER, Blue RE, Tsai Y-H, Combs M, Davi J, Coffey AR, Boriek AM, Taylor JM, Parker JS & Giudice J (2022) Stretching muscle cells induces transcriptional and splicing transitions and changes in SR proteins. *Commun Biol* 5: 987

Hood DA, Tryon LD, Carter HN, Kim Y & Chen CCW (2016) Unravelling the mechanisms regulating muscle mitochondrial biogenesis. *Biochem J* 473: 2295–2314

Horibata Y, Ando H, Itoh M & Sugimoto H (2013) Enzymatic and transcriptional regulation of the cytoplasmic acetyl-CoA hydrolase ACOT12. *J Lipid Res* 54: 2049–2059

Hulmi JJ, Ahtiainen JP, Kaasalainen T, Pöllänen E, Häkkinen K, Alen M, Selänne H, Kovanen V & Mero AA (2007) Postexercise myostatin and activin IIb mRNA levels: effects of strength training. *Med Sci Sports Exerc* 39: 289–297

Ilaiwy A, Quintana MT, Bain JR, Muehlbauer MJ, Brown DI, Stansfield WE & Willis MS (2016) Cessation of biomechanical stretch model of C2C12 cells models myocyte atrophy and anaplerotic changes in metabolism using non-targeted metabolomics analysis. *Int J Biochem Cell Biol* 79: 80–92

Jing X, Lyu J & Xiong J (2023) Acetate regulates GAPDH acetylation and T helper 1 cell differentiation. *Mol Biol Cell* 34: br10

Jufri NF, Mohamedali A, Avolio A & Baker MS (2015) Mechanical stretch: physiological and pathological implications for human vascular endothelial cells. *Vasc Cell* 7: 8

Kim J, Cross JM & Bamman MM (2005) Impact of resistance loading on myostatin expression and cell cycle regulation in young and older men and women. *Am J Physiol Endocrinol Metab* 288: E1110-1119

Kobialka P & Graupera M (2019) Revisiting PI3-kinase signalling in angiogenesis. *Vasc Biol Bristol Engl* 1: H125–H134

Kong X, Kapustka A, Sullivan B, Schwarz GJ & Leckband DE (2022) Extracellular matrix regulates force transduction at VE-cadherin junctions. *Mol Biol Cell* 33: ar95

Kujala UM, Mäkinen V-P, Heinonen I, Soininen P, Kangas AJ, Leskinen TH, Rahkila P, Würtz P, Kovanen V, Cheng S, *et al* (2013) Long-term leisure-time physical activity and serum metabolome. *Circulation* 127: 340–348

Kwee BJ, Budina E, Najibi AJ & Mooney DJ (2018) CD4 T-cells regulate angiogenesis and myogenesis. *Biomaterials* 178: 109–121

Langmead B & Salzberg SL (2012) Fast gapped-read alignment with Bowtie 2. *Nat Methods* 9: 357–359

Lautaoja JH, M O'Connell T, Mäntyselkä S, Peräkylä J, Kainulainen H, Pekkala S, Permi P & Hulmi JJ (2021) Higher glucose availability augments the metabolic responses of the C2C12 myotubes to exercise-like electrical pulse stimulation. *Am J Physiol Endocrinol Metab* 321: E229–E245

Lautaoja JH, Turner DC, Sharples AP, Kivelä R, Pekkala S, Hulmi JJ & Ylä-Outinen L (2023) Mimicking exercise in vitro: effects of myotube contractions and mechanical stretch on omics. *Am J Physiol Cell Physiol* 324: C886–C892

Law CW, Chen Y, Shi W & Smyth GK (2014) voom: Precision weights unlock linear model analysis tools for RNA-seq read counts. *Genome Biol* 15: R29

Lee G, Wong C, Cho A, West JJ, Crawford AJ, Russo GC, Si BR, Kim J, Hoffner L, Jang C, *et al* (2024) E-Cadherin Induces Serine Synthesis to Support Progression and Metastasis of Breast Cancer. *Cancer Res* 84: 2820–2835

Legrand C, Bour JM, Jacob C, Capiaumont J, Martial A, Marc A, Wudtke M, Kretzmer G, Demangel C & Duval D (1992) Lactate dehydrogenase (LDH) activity of the cultured eukaryotic cells as marker of the number of dead cells in the medium [corrected]. *J Biotechnol* 25: 231–243

Li S, Xu Z, Wang Y, Chen L, Wang X, Zhou Y, Lei D, Zang G & Wang G (2024) Recent advances of mechanosensitive genes in vascular endothelial cells for the formation and treatment of atherosclerosis. *Genes Dis* 11: 101046

Li W & Sumpio BE (2005) Strain-induced vascular endothelial cell proliferation requires PI3K-dependent mTOR-4E-BP1 signal pathway. *Am J Physiol Heart Circ Physiol* 288: H1591-1597

Liao Y, Smyth GK & Shi W (2014) featureCounts: an efficient general purpose program for assigning sequence reads to genomic features. *Bioinforma Oxf Engl* 30: 923–930

Liu X, Cooper DE, Cluntun AA, Warmoes MO, Zhao S, Reid MA, Liu J, Lund PJ, Lopes M, Garcia BA, *et al* (2018) Acetate Production from Glucose and Coupling to Mitochondrial Metabolism in Mammals. *Cell* 175: 502-513.e13

Lorenz L, Axnick J, Buschmann T, Henning C, Urner S, Fang S, Nurmi H, Eichhorst N, Holtmeier R, Bódis K, *et al* (2018) Mechanosensing by β1 integrin induces angiocrine signals for liver growth and survival. *Nature* 562: 128–132

Lunt SY & Vander Heiden MG (2011) Aerobic glycolysis: meeting the metabolic requirements of cell proliferation. *Annu Rev Cell Dev Biol* 27: 441–464

Manning BD & Toker A (2017) AKT/PKB Signaling: Navigating the Network. *Cell* 169: 381–405

Mäntyselkä S, Kolari K, Baumert P, Ylä-Outinen L, Kuikka L, Lahtonen S, Permi P, Wackerhage H, Kalenius E, Kivelä R, *et al* (2024) Serine synthesis pathway

enzyme PHGDH is critical for muscle cell biomass, anabolic metabolism, and mTORC1 signaling. *Am J Physiol Endocrinol Metab* 326: E73–E91

Millard P, Delépine B, Guionnet M, Heuillet M, Bellvert F & Létisse F (2019) IsoCor: isotope correction for high-resolution MS labeling experiments. *Bioinforma Oxf Engl* 35: 4484–4487

Miller KD, O'Connor S, Pniewski KA, Kannan T, Acosta R, Mirji G, Papp S, Hulse M, Mukha D, Hlavaty SI, *et al* (2023) Acetate acts as a metabolic immunomodulator by bolstering T-cell effector function and potentiating antitumor immunity in breast cancer. *Nat Cancer* 4: 1491–1507

Nakai N, Kawano F & Nakata K (2015) Mechanical stretch activates mammalian target of rapamycin and AMP-activated protein kinase pathways in skeletal muscle cells. *Mol Cell Biochem* 406: 285–292

Nan W, He Y, Wang S & Zhang Y (2023) Molecular mechanism of VE-cadherin in regulating endothelial cell behaviour during angiogenesis. *Front Physiol* 14: 1234104

Pacold ME, Brimacombe KR, Chan SH, Rohde JM, Lewis CA, Swier LJYM, Possemato R, Chen WW, Sullivan LB, Fiske BP, *et al* (2016) A PHGDH inhibitor reveals coordination of serine synthesis and one-carbon unit fate. *Nat Chem Biol* 12: 452–458

Peng Z, Shu B, Zhang Y & Wang M (2019) Endothelial Response to Pathophysiological Stress. *Arterioscler Thromb Vasc Biol* 39: e233–e243

Pepe GJ & Albrecht ED (2023) Microvascular Skeletal-Muscle Crosstalk in Health and Disease. *Int J Mol Sci* 24: 10425

Pillon NJ, Gabriel BM, Dollet L, Smith JAB, Sardón Puig L, Botella J, Bishop DJ, Krook A & Zierath JR (2020) Transcriptomic profiling of skeletal muscle adaptations to exercise and inactivity. *Nat Commun* 11: 470

Powers SK, Radak Z, Ji LL & Jackson M (2024) Reactive oxygen species promote endurance exercise-induced adaptations in skeletal muscles. *J Sport Health Sci* 13: 780–792

Qasem RJ, Farh IK & Al Essa MA (2017) A novel LC-MS/MS method for the quantitative measurement of the acetate content in pharmaceutical peptides. *J Pharm Biomed Anal* 146: 354–360

Qiu J, Villa M, Sanin DE, Buck MD, O'Sullivan D, Ching R, Matsushita M, Grzes KM, Winkler F, Chang C-H, *et al* (2019) Acetate Promotes T Cell Effector Function during Glucose Restriction. *Cell Rep* 27: 2063-2074.e5

Ren D, Song J, Liu R, Zeng X, Yan X, Zhang Q & Yuan X (2021) Molecular and Biomechanical Adaptations to Mechanical Stretch in Cultured Myotubes. *Front Physiol* 12: 689492

Ritchie ME, Phipson B, Wu D, Hu Y, Law CW, Shi W & Smyth GK (2015) limma powers differential expression analyses for RNA-sequencing and microarray studies. *Nucleic Acids Res* 43: e47

Robinson MD, McCarthy DJ & Smyth GK (2010) edgeR: a Bioconductor package for differential expression analysis of digital gene expression data. *Bioinforma Oxf Engl* 26: 139–140

Robinson MD & Oshlack A (2010) A scaling normalization method for differential expression analysis of RNA-seq data. *Genome Biol* 11: R25

Ross M, Kargl CK, Ferguson R, Gavin TP & Hellsten Y (2023) Exercise-induced skeletal muscle angiogenesis: impact of age, sex, angiocrines and cellular mediators. *Eur J Appl Physiol* 123: 1415–1432

Schiaffino S, Pereira MG, Ciciliot S & Rovere-Querini P (2017) Regulatory T cells and skeletal muscle regeneration. *FEBS J* 284: 517–524

Schranner D, Kastenmüller G, Schönfelder M, Römisch-Margl W & Wackerhage H (2020) Metabolite Concentration Changes in Humans After a Bout of Exercise: a Systematic Review of Exercise Metabolomics Studies. *Sports Med - Open* 6: 11

Seo H-R, Jeong HE, Joo HJ, Choi S-C, Park C-Y, Kim J-H, Choi J-H, Cui L-H, Hong SJ, Chung S, *et al* (2016) Intrinsic FGF2 and FGF5 promotes angiogenesis of human aortic endothelial cells in 3D microfluidic angiogenesis system. *Sci Rep* 6: 28832

Smith JAB, Gabriel BM, Abdelmoez AM, Savikj M, Wright SC, Koutsilieri S, Barrès R, Lauschke VM, Krook A, Zierath JR, *et al* (2024) Downregulation of NR4A3 during inactivity alters glucose metabolism and impairs translation in human skeletal muscle. doi:10.1101/2024.03.11.584422 [PREPRINT]

Smith JAB, Murach KA, Dyar KA & Zierath JR (2023) Exercise metabolism and adaptation in skeletal muscle. *Nat Rev Mol Cell Biol* 24: 607–632

Sottiurai VS, Sue SL, Breaux JR & Smith LM (1989) Adaptability of endothelial orientation to blood flow dynamics--a morphologic analysis. *Eur J Vasc Surg* 3: 145–151

Stegen S, Loopmans S, Stockmans I, Moermans K, Carmeliet P & Carmeliet G (2022) De novo serine synthesis regulates chondrocyte proliferation during bone development and repair. *Bone Res* 10: 14

Tsugawa H, Kanazawa M, Ogiwara A & Arita M (2014) MRMPROBS suite for metabolomics using large-scale MRM assays. *Bioinforma Oxf Engl* 30: 2379–2380

Turner DC, Gorski PP, Seaborne RA, Viggars M, Murphy M, Jarvis JC, Martin NRW, Stewart CE & Sharples AP (2021) Mechanical loading of bioengineered skeletal muscle in vitro recapitulates gene expression signatures of resistance exercise in vivo. *J Cell Physiol* 236: 6534–6547

Vandekeere S, Dubois C, Kalucka J, Sullivan MR, García-Caballero M, Goveia J, Chen R, Diehl FF, Bar-Lev L, Souffreau J, *et al* (2018) Serine Synthesis via PHGDH Is Essential for Heme Production in Endothelial Cells. *Cell Metab* 28: 573-587.e13

Verma M, Asakura Y, Murakonda BSR, Pengo T, Latroche C, Chazaud B, McLoon LK & Asakura A (2018) Muscle Satellite Cell Cross-Talk with a Vascular Niche maintains quiescence via VEGF and Notch Signaling. *Cell Stem Cell* 23: 530-543.e9

Wickramasinghe NM, Sachs D, Shewale B, Gonzalez DM, Dhanan-Krishnan P, Torre D, LaMarca E, Raimo S, Dariolli R, Serasinghe MN, *et al* (2022) PPARdelta activation induces metabolic and contractile maturation of human pluripotent stem cell-derived cardiomyocytes. *Cell Stem Cell* 29: 559-576.e7

Yoon SJ, Combs JA, Falzone A, Prieto-Farigua N, Caldwell S, Ackerman HD, Flores ER & DeNicola GM (2023) Comprehensive Metabolic Tracing Reveals the Origin and Catabolism of Cysteine in Mammalian Tissues and Tumors. *Cancer Res* 83: 1426–1442

Yu G, Wang L-G, Han Y & He Q-Y (2012) clusterProfiler: an R package for comparing biological themes among gene clusters. *Omics J Integr Biol* 16: 284–287

Yung YC, Chae J, Buehler MJ, Hunter CP & Mooney DJ (2009) Cyclic tensile strain triggers a sequence of autocrine and paracrine signaling to regulate angiogenic sprouting in human vascular cells. *Proc Natl Acad Sci U S A* 106: 15279–15284

Zhang D, Li AM, Hu G, Huang M, Yang F, Zhang L, Wellen KE, Xu X, Conn CS, Zou W, *et al* (2023) PHGDH-mediated endothelial metabolism drives glioblastoma resistance to chimeric antigen receptor T cell immunotherapy. *Cell Metab* 35: 517-534.e8

Zhang T, Gillies MC, Madigan MC, Shen W, Du J, Grünert U, Zhou F, Yam M & Zhu L (2018) Disruption of De Novo Serine Synthesis in Müller Cells Induced Mitochondrial Dysfunction and Aggravated Oxidative Damage. *Mol Neurobiol* 55: 7025–7037

Zhang X, Sun M, Jiao Y, Lin B & Yang Q (2022) PHGDH Inhibitor CBR-5884 Inhibits Epithelial Ovarian Cancer Progression via ROS/Wnt/β-Catenin Pathway and Plays a Synergistic Role with PARP Inhibitor Olaparib. *Oxid Med Cell Longev* 2022: 9029544